A Photometric Study of the Eclipsing Binary Star PY Boötis

Edward J. Michaels
Stephen F. Austin State University, Department of Physics and Astronomy, P.O. Box 13044, Nacogdoches, TX 75962; emichaels@sfasu.edu

Received August 27, 2016; revised October 3, 2016; accepted October 3, 2016

Abstract Presented here are the first precision multi-band CCD photometry of the eclipsing binary star PY Boötis. Best-fit stellar models were determined by analyzing the light curves with the Wilson-Devinney program. Asymmetries in the light curves were interpreted as resulting from magnetic activity which required spots to be included in the model. The resulting model is consistent with a W-type contact eclipsing binary having total eclipses.

1. Introduction

PY Boötis (GSC 3488-0585) was first identified as a contact binary from the sky patrol data taken by the ROTSE-I telescope (Gettel *et al.* 2006). The orbital period was given as 0.278045 day, a maximum and minimum visual magnitude of 12.09 and 12.67, and an estimated distance of 182 pc. This star was also identified by Hoffman *et al.* (2009) in the Northern Sky Variability Survey (NSVS; Wozniak *et al.* 2004). The Large Sky Area Multi-Object Fiber Spectroscopic Telescope (LAMOST) survey gives a spectral type of K3, a metallicity of [Fe/H] = –0.185, a heliocentric radial velocity of V_r = –68.81 km/sec, and surface gravity of log g = 4.1351 (cgs) (Luo *et al.* 2015). Several observers have reported times of minima for primary and secondary eclipses (see section 3).

In this paper, the first photometric study of PY Boo is presented. The paper is organized as follows. The observations and data reduction methods are presented in section 2. New times of minima and period analysis are presented in section 3. Analysis of the light curves using Binary Maker 3.0 (BM3; Bradstreet and Steelman 2002) and the Wilson-Devinney (WD; 1971) model is presented in section 4. Discussion of the results and conclusions are presented in section 5.

2. Observations

Photometric data for PY Boo were acquired with the 0.31-m Ritchey-Chretien robotic telescope at the Waffelow Creek Observatory (http://obs.ejmj.net/index.php). The imaging camera was a SBIG-STXL model equipped with a cooled KAF-6303E CCD (–30°C). Images were acquired on the following nights in 2016: March 13, 14, and 28, April 2, 3, 4, and 6. A total of 1,736 filtered images were taken in three Sloan passbands, 395 in g', 816 in r', and 525 in i'. This set of images was used in the light curve analysis of section 4. Additional images were acquired on April 21, 25, and 29, May 1, 3, and 31, June 3, 4,

Table 1. Stars used in this study.

Star	*R.A. (2000) h m s*	*Dec. (2000) ° ′ ″*	*g′*	*r′*	*i′*	*B–V*
PY Boo	15 28 22	+51 32 22				
GSC 3488-0933 (C1)	15 27 43	+51 22 51	11.756 ± 0.100	11.098 ± 0.073	10.838 ± 0.105	0.885 ± 0.108
GSC 3488-0648 (C2)	15 29 15	+51 30 27	12.212 ± 0.062	11.425 ± 0.040	11.047 ± 0.056	1.062 ± 0.072
GSC 3488-0033 (C3)	15 29 29	+51 41 59	12.894 ± 0.057	12.214 ± 0.045	11.889 ± 0.059	0.956 ± 0.059
GSC 3488-0559 (C4)	15 29 08	+51 33 27	13.346 ± 0.061	12.583 ± 0.040	12.194 ± 0.057	1.016 ± 0.075
GSC 3488-0473 (C5)	15 28 14	+51 36 30	13.512 ± 0.117	12.896 ± 0.073	12.618 ± 0.099	0.842 ± 0.111
GSC 3488-0014 (K)	15 28 10	+51 40 31	12.195 ± 0.103	11.761 ± 0.039	11.610 ± 0.080	0.664 ± 0.078
Observed check star magnitudes (K)			12.136 ± 0.037	11.753 ± 0.025	11.597 ± 0.035	
Standard Deviation of check star magnitudes (K)			± 0.006	± 0.005	± 0.006	

APASS comparison stars (C1–C5) and check (K) star magnitudes.

Table 2. Available times of minima and O–C residuals from Equation (2).

Epoch HJD 2400000+	*Error*	*Cycle*	*O–C Linear*	*References*
56029.86060	0.00050	0.0	0.00000	Diethelm 2012
56060.44490	0.00020	110.0	–0.00109	Hübscher 2013a
56400.49990	0.00480	1333.0	–0.00002	Hübscher 2013b
56407.45179	0.00006	1358.0	0.00065	Hoňková *et al.* 2014
56745.55690	0.00140	2574.0	–0.00183	Hübscher 2015a
57066.70370	0.00010	3729.0	–0.00162	Hübscher 2015b
57123.42540	0.00010	3933.0	–0.00192	Hübscher 2016
57134.82516	0.00003	3974.0	–0.00217	this paper
57142.88823	0.00006	4003.0	–0.00252	this paper
57146.78135	0.00006	4017.0	–0.00208	this paper
57174.86354	0.00007	4118.0	–0.00284	this paper
57179.86843	0.00003	4136.0	–0.00283	this paper
57180.70279	0.00002	4139.0	–0.00262	this paper
57185.70745	0.00005	4157.0	–0.00284	this paper
57461.80761	0.00005	5150.0	–0.00534	this paper
57481.82709	0.00005	5222.0	–0.00539	this paper
57483.77344	0.00006	5229.0	–0.00538	this paper
57485.71973	0.00004	5236.0	–0.00543	this paper
57513.80272	0.00009	5337.0	–0.00539	this paper
57514.63659	0.00008	5340.0	–0.00567	this paper

5, and 6, and July 12, 13, 14, and 15 in 2015 and May 4 and 5 in 2016. These additional images were used primarily for new times of minima but also proved useful in monitoring changes in the light curves over the course of one year. All light images were calibrated with bias, dark, and flat field frames. The calibration and ensemble differential aperture photometry was accomplished using MIRA software (Mirametrics 2015). Table 1 lists the comparison and check stars used in this study with a finder chart shown in Figure 1. The instrumental magnitudes of PY Boo were converted to standard magnitudes using the comparison star magnitudes from the AAVSO Photometric All-Sky Survey (APASS; Henden *et al.* 2014). The Heliocentric Julian Date (HJD) of each observation was converted to orbital phase using an epoch of T_0 = 2457514.6366 and an orbital period of P = 0.27804651. All light curves in this paper were plotted from phase –0.6 to 0.6 with negative phase defined by φ – 1. The folded light curves of the observations are shown in Figure 2 with the r' passband check star observations shown in the bottom panel. The check star magnitudes were inspected each night and no significant variability was found. The observations in this study are accessible from the AAVSO International Database (Kafka 2015).

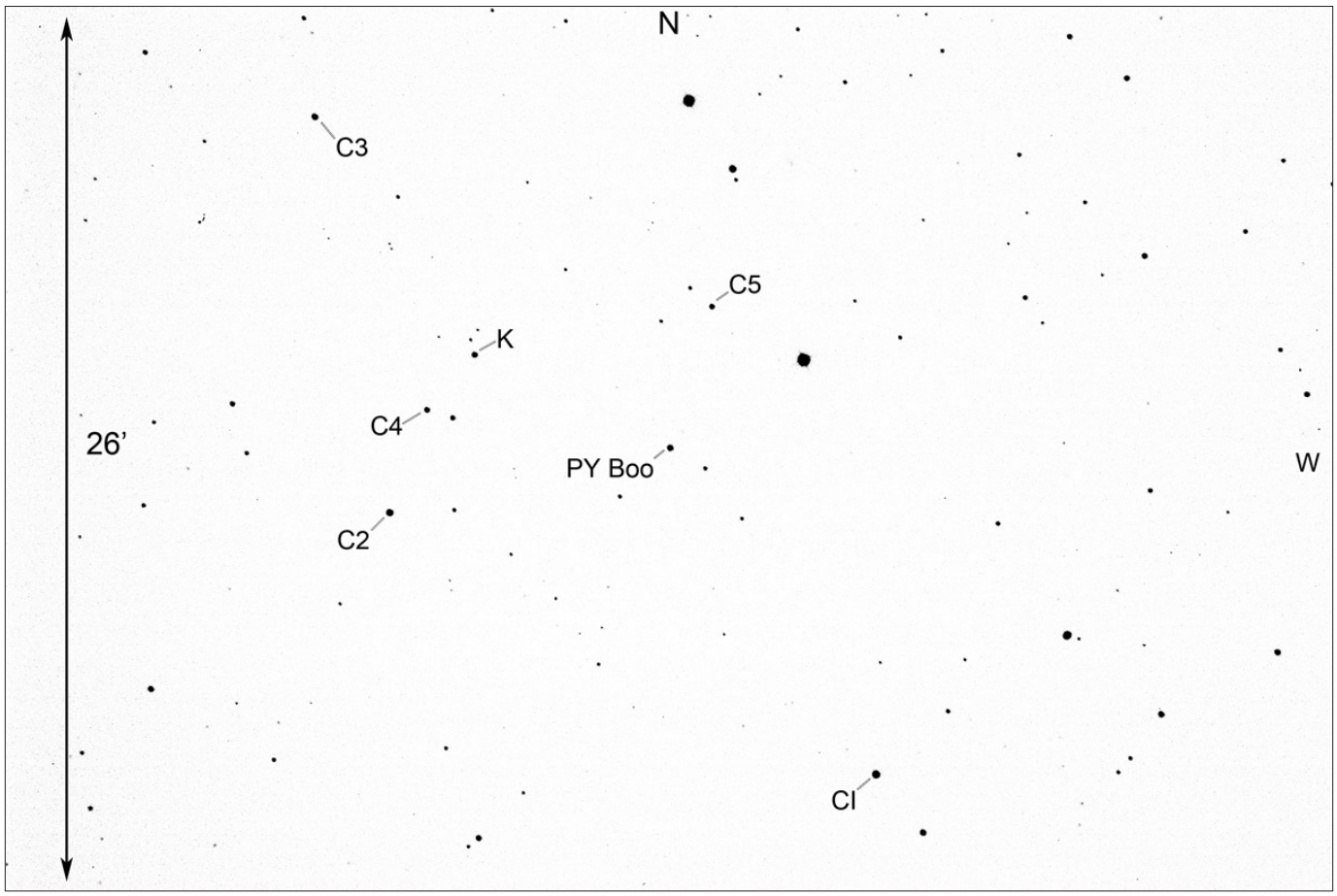

Figure 1. Finder chart for PY Boo, comparison stars (C1–C7), and the check (K) star.

3. Period study and ephemerides

From the observations the HJD for 13 new times of primary minima were determined. These new minima times along with all others found in the literature are collected in Table 2. The initial linear ephemeris for this study (Equation 1 below) contains the period from Paschke (2014) and the epoch from a primary minima reported by Deithelm (2012).

$$\text{HJD Min I} = 2456029.8606 + 0.278049\ E. \quad (1)$$

The residuals from Equation 1 were used to calculate a new linear ephemeris by least squares solution and is given by

$$\text{HJD Min I} = 2457514.6377\ (6) + 0.27804797\ (14)\ E. \quad (2)$$

The residuals from Equation 1 and the best-fit linear line of Equation 2 are shown in the Figure 3 ephemeris diagram. The general trend of the O–C residuals indicates the orbital period is continuously decreasing. A second least-squares solution of the residuals from Equation 2 yields the following quadratic ephemeris:

$$\text{HJD Min I} = 2457514.6416\ (3) + 0.27804620\ (24)\ E - 2.50\ (30) \times 10^{-9}\ E2. \quad (3)$$

Figure 4 shows the quadratic ephemeris (solid line) is an improved fit to the residuals compared to the linear solution. The rate of period change from this solution gives a value of $dP / dt = -9.13\ (1.08) \times 10^{-7}$ d yr^{-1}. Compared to other binaries of this type, this period change is quite rapid and will be discussed further in section 5.

4. Analysis

4.1. Temperature, spectral type

The effective temperature and spectral type were estimated from the observed (g'-r') color index and Jester's (2005) transformation equation,

$$(B–V) = \frac{(g' – r') + 0.23}{1.09}. \quad (4)$$

The phase and magnitude of the g' and r' observations were binned with a phase width of 0.01. The phases and magnitudes in each bin interval were averaged. The binned r' magnitudes were subtracted from the linearly interpolated g' magnitudes at primary eclipse ($\varphi = \pm 0.035$) which gives a (g' – r') value of 0.791 ± 0.018. Figure 5 shows the binned r' magnitude light curve with the bottom panel showing the (g' – r') color index. Using Equation 4 gives a (B–V) color of 0.937 ± 0.040. To correct for interstellar reddening, the Willingale *et al.* (2013) method based on the galactic column density of hydrogen was used. The galactic coordinates for this star gave a color excess of E(B–V) = 0.017 and a corrected color of (B–V) = 0.920. Using Table 5 of Pecaut and Mamajek (2013) gives an effective temperature of 4984 ± 82 K and a spectral type of K3. This

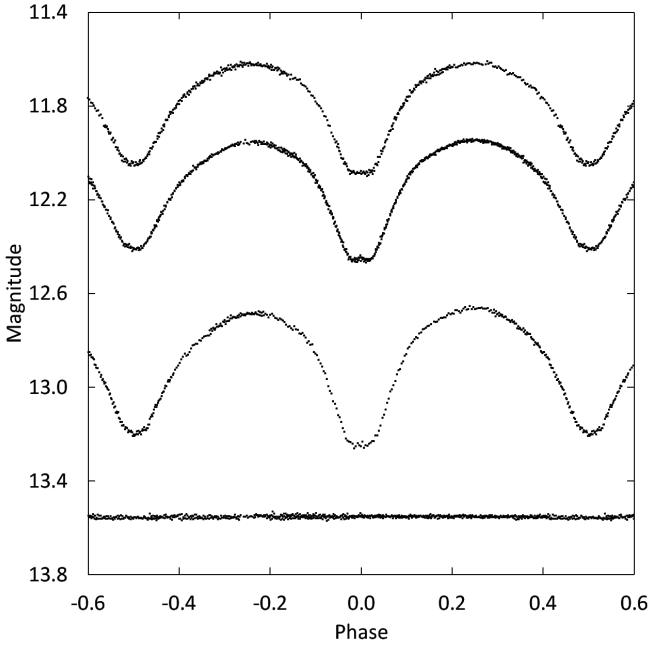

Figure 2. Folded light curves for each observed passband. The differential magnitudes of the variable were converted to standard magnitudes using the calibrated magnitudes of the comparison stars. From top to bottom the light curve passbands are Sloan i', Sloan r', Sloan g'. The bottom curve shows the Sloan r' magnitudes of the check star (offset +1.8 magnitudes). The standard deviations of check star magnitudes (all nights) are shown in Table 1. Error bars are not shown for clarity.

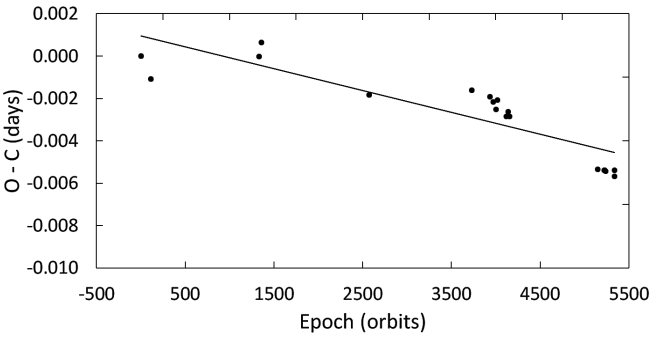

Figure 3. O–C residuals from Equation (1) with the solid line the linear ephemeris fit of Equation (2).

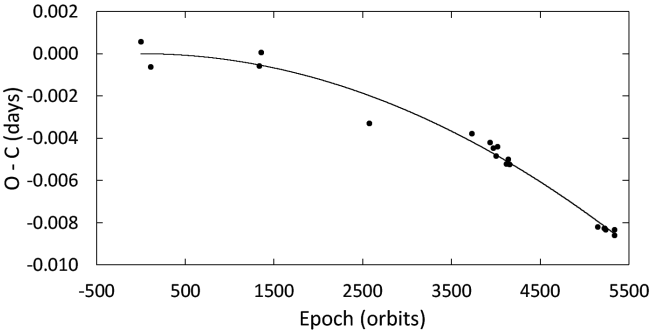

Figure 4. O–C residuals from Equation (2) with the solid line the quadratic ephemeris fit of Equation (3).

temperature was determined from the color at primary eclipse. Since the eclipse is total, only light from the larger secondary star was measured. This effective temperature will be assigned to the secondary star in the light curve analysis of section 4.2.

4.2. Synthetic light curve modeling

The Sloan g', r', and i' observations from March 13 to April 6, 2016, were used for the light curve modeling. The observations were binned in both phase and magnitude with a phase interval of 0.01. The average number of observations per bin was 6. The binned magnitudes were converted to relative flux for modeling. BINARY MAKER 3.0 (BM3) (Bradstreet and Steelman 2002) was used to make preliminary fits to each light curve. Standard convective parameters and limb darkening coefficients from Van Hamme's (1993) tabular values were utilized in the model. Obtaining a reasonably good fit required a third light contribution in all three passbands. There was also a noticeable asymmetry in the secondary eclipse of each light curve. The fit between the observed flux and the synthetic light curve showed a loss of light from phase φ = 0.51 to φ = 0.83, possibly caused by a dark spot on the secondary star. Since the initial BM3 light curve fits and the first WD solution attempt would not incorporate spots in the model, it was decided not to use observations from this phase range. With the observations for this phase range removed the synthetic BM3 light curve for each color fit well and was consistent. The resulting stellar parameter values from each light curve fit were averaged and used as the initial input parameters for computation of a simultaneous three-color light curve solution with the WD program (Wilson and Devinney 1971; Van Hamme and Wilson 1998). The light curve morphology is characteristic of a W-type eclipsing binary, therefore a common convective envelope was assumed and Mode 3 was set in the program. The weight assigned to each input data point was set to the number of observations that formed that point. To minimize strong correlations of the parameters, the Method of Multiple Subsets (MMS) (Wilson and Biermann 1976) was employed. The Kurucz stellar atmosphere model was applied and the fixed inputs included standard convective parameters: gravity darkening, $g_1 = g_2 = 0.32$ (Lucy 1968) and albedo value $A_1 = A_2 = 0.5$ (Ruciński 1969). The temperature of the cooler secondary star, T_2, was fixed at the value determined in section 4.1, 4984 K. Linear limb darkening coefficients were calculated by the program from tabulated values using the method of Van Hamme (1993). The solution's adjustable parameters include the inclination (i), mass ratio ($q = M_2 / M_1$), potential ($\Omega_1 = \Omega_2$), temperature of the primary star (T_1), the normalized flux for each wavelength (L), and third light (ℓ). The best-fit solution parameters with errors are shown in column 2 of Table 3 (Solution 1). The fill-out was computed using a modification of the parameter defined by Lucy and Wilson (1979) and is given by

$$f = \frac{(\Omega_{inner} - \Omega)}{(\Omega_{inner} - \Omega_{outer})}, \quad (5)$$

where Ω_{inner} and Ω_{outer} are the inner and outer critical equipotential surfaces that pass through the Lagrangian points L_1 and L_2

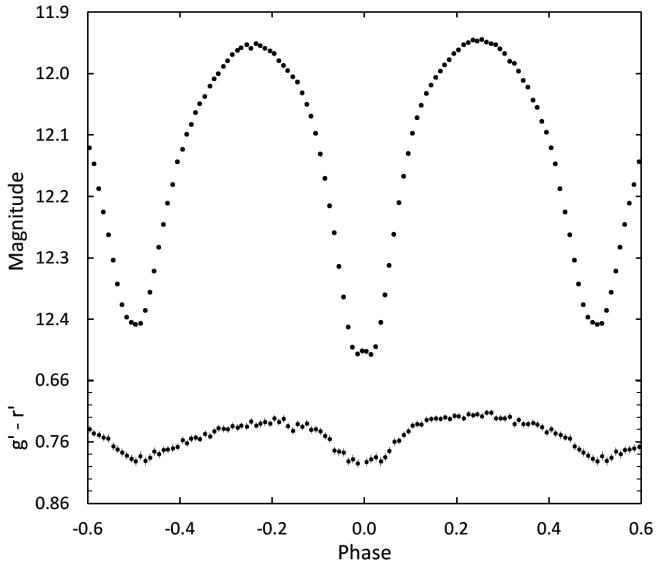

Figure 5. Light curve of all r'-band observations are in standard magnitudes (top panel). The observations were binned with a phase width of 0.01. The errors for each binned point are about the size of the plotted points. The g'–r' colors were calculated by subtracting the binned Sloan g' magnitudes from the linearly interpolated binned Sloan r' magnitudes.

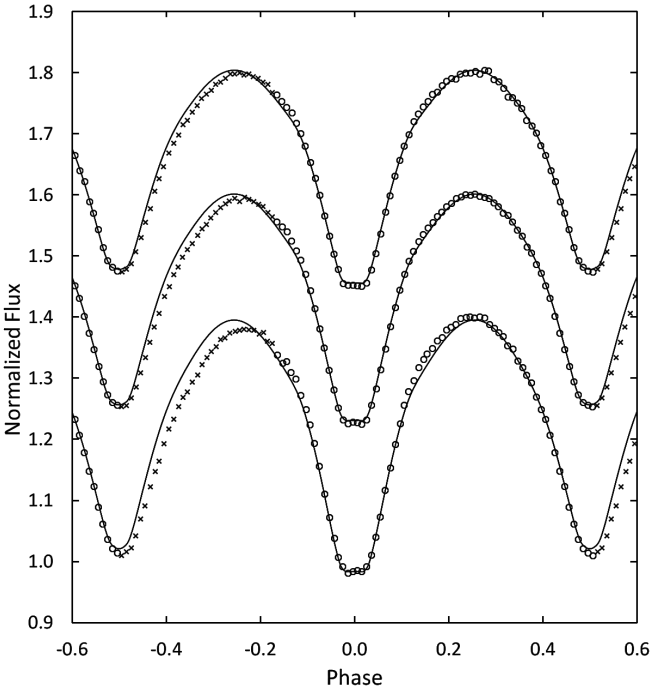

Figure 6. The WD model fit without spots (solid curve) to the observed normalized flux curves for each passband. For the data points plotted, the circles are the observations that were used in this solution and the crosses are the observations (phase 0.51–0.83) not used. From top to bottom the passbands are Sloan i', Sloan r', and Sloan g'. Each curve is offset by 0.2 for this combined plot. The best-fit parameters are given in column 2 of Table 3. Error bars are omitted from the points for clarity.

Table 3. PY Boo synthetic light curve solutions.

Parameter	*Solution 1 (no spots)*	*Solution 2 (with spots)*	*Solution 3 (g′ light curve only)*
phase shift	–0.0005 ± 0.0001	0.0000 ± 0.0001	[3] 0.0000 ± 0.0002
i (°)	89 ± 2	90 ± 3	[3] 90 ± 4
T_1 (K)	5248 ± 5	5254 ± 27	[3] 5254 ± 31
T_2 (K)	[1]4984	[1]4984	[1] 4984
$\Omega_1 = \Omega_2$	5.45 ± 0.02	5.46 ± 0.02	[3] 5.46 ± 0.02
$q(M_2 / M_1)$	2.22 ± 0.02	2.20 ± 0.01	[3] 2.20 ± 0.02
filling factor	17%	12%	[3] 12%
$L_1 / (L_1 + L_2)$ (g')	0.406 ± 0.001	0.409 ± 0.003	0.409 ± 0.002
$L_1 / (L_1 + L_2)$ (r')	0.385 ± 0.001	0.387 ± 0.002	—
$L_1 / (L_1 + L_2)$ (i')	0.376 ± 0.001	0.378 ± 0.001	—
[2]ℓ_3 (g')	0.210 ± 0.004	0.211 ± 0.010	0.210 ± 0.017
[2]ℓ_3 *(r')*	0.247 ± 0.004	0.248 ± 0.008	—
[2]ℓ_3 *(i')*	0.272 ± 0.004	0.273 ± 0.007	—
r_1 side	0.316 ± 0.001	0.311 ± 0.001	0.314 ± 0.001
r_2 side	0.436 ± 0.003	0.466 ± 0.002	0.468 ± 0.003
pot parameters		*Star 1 – Hot Spot*	*Star 1 – Hot Spot*
colatitude (°)	—	81 ± 9	85 ± 7
longitude (°)	—	0.0 ± 0.3	359.0 ± 0.6
spot radius (°)	—	15 ± 3	15 ± 3
temp.– factor	—	1.3 ± 0.1	1.3 ± 0.1
		Star 2 – Cool Spot	*Star 2 – Cool Spot*
colatitude (°)	—	62 ± 8	60 ± 11
longitude (°)	—	346 ± 3	337 ± 6
spot radius (°)	—	22 ± 6	26 ± 6
temp.– factor	—	0.89 ± 0.04	0.89 ± 0.04

[1] *Assumed.*
[2] *Third lights are the percent of light contributed at orbital phase 0.25.*
[3] *These parameters were fixed at the spotted Solution 2 values.*

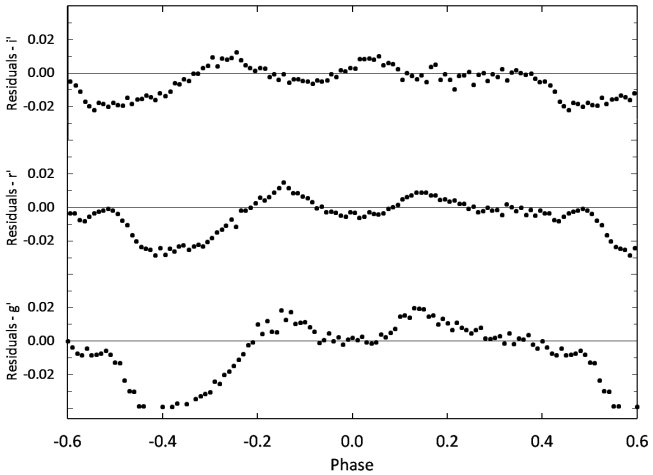

Figure 7. The residuals for the best-fit WD model without spots. Error bars are omitted from the points for clarity.

and Ω is the equipotential surface which describes the stellar surface. For this solution $\Omega_{inner} = 5.55$, $\Omega_{outer} = 4.95$, and $\Omega = 5.45$, which gives a fill-out value of f = 0.17 which indicates a contact system. The normalized light curves for each passband, overlaid by the synthetic solution curves, are shown in Figure 6 with the residuals shown in Figure 7.

4.3. Spot model

Low mass short period contact binaries are often magnetically active and therefore spotted. The asymmetries in the light curves seen in Figure 6 are most likely due to cool spots and hot regions such as faculae on the star surfaces. A new spot model was attempted but this time the entire phase range of observations was used for modeling in both BM3 and the WD program. As noted earlier, compared to the synthetic light curves, the observations show a light loss between phase φ = 0.51 and φ = 0.83 (see Figure 6). This indicates a possible under-luminous region (cool spot) on the larger secondary star. The residuals of Figure 7 also indicate excess light symmetrically located on either side of primary eclipse. The location of this excess light could be explained by an over-luminous region (hot spot) on the smaller primary star close to the line of centers between the two stars. It is important to note with an inclination close to i = 90°, the spots could be located either above or below the contact point and give essentially the same results. Two spots were therefore modeled

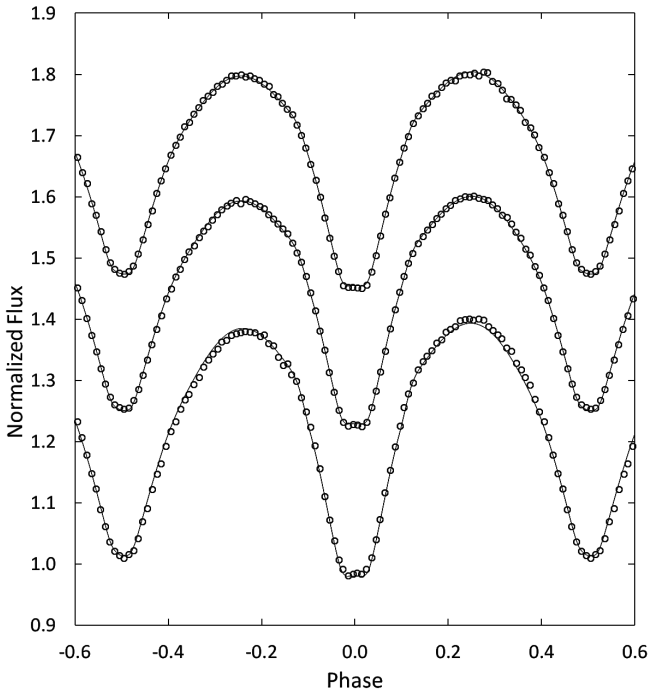

Figure 8. The WD model fit with spots (solid curve) to the observed normalized flux curves for each passband. From top to bottom the passbands are Sloan i', Sloan r', and Sloan g'. Each curve is offset by 0.2 for this combined plot. The best-fit parameters are given in column 3 of Table 3. Error bars are omitted from the points for clarity.

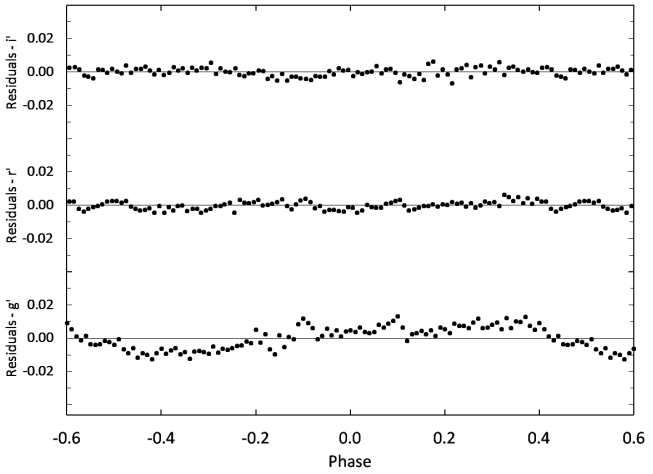

Figure 9. The residuals for the spotted WD model in each passband. Error bars are omitted from the points for clarity.

with BM3. Each spot's parameters (latitude, longitude, spot size, and temperature) were adjusted until a good fit resulted between the synthetic and observed light curves. The best-fit spot parameters from BM3 were then incorporated into a new WD solution attempt. Initially the stellar parameters were held fixed with only the light and spot parameters adjusted until the solution converged. At this point the spot parameters were held fixed and the stellar parameters adjusted until the solution converged again. This process was repeated until the model converged to a final solution. The best-fit WD spotted solution model is shown in column 3 of Table 3 (Solution 2). Figure 8 shows the final spotted model fit (solid line) to the observed light curves and Figure 9 the residuals. A graphical representation of the spotted model is shown in Figure 10.

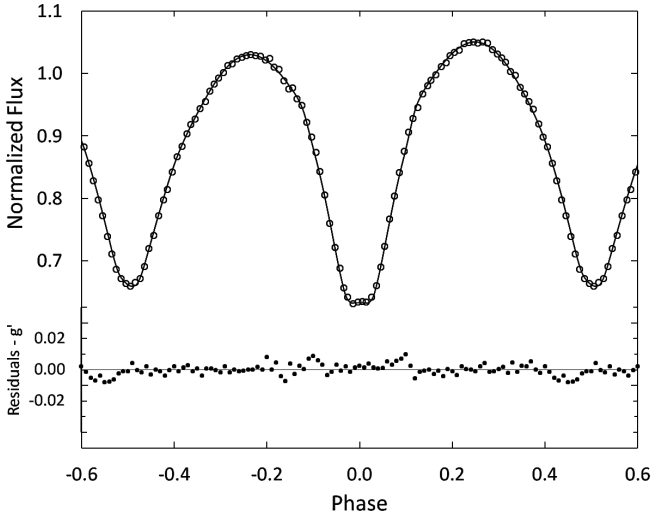

Figure 10. The WD model fit with spots (solid curve) to the observed normalized flux curves for Sloan g' passband. The residuals are shown in the bottom panel. The best-fit parameters are given in column 4 of Table 3. Error bars are omitted from the points for clarity.

5. Discussion and conclusions

PY Boo is a member of the W-type subclass of eclipsing binaries. Its more massive and cooler secondary star has a lower surface brightness than its companion and primary minimum is an occultation. The best-fit WD spotted solution with a fill-out value of 12% is consistent with a contact binary. The total eclipses provide the necessary constraints to calculate provisional absolute stellar parameters for the stars (Wilson 1978; Terrell and Wilson 2005). The secondary star's mass can be estimated from the orbital period using an empirical relationship derived by Qian's (2003) statistical study of contact systems. Using the orbital period in this relationship,

$$M_2 = 0.391\ (\pm 0.059) + 1.96\ (\pm 0.17)\ P, \qquad (6)$$

gives a mass for the secondary star of $M_2 = 0.94 \pm 0.06\ M_\odot$. Using the mass ratio from the WD spotted solution gives a primary star mass of $M_1 = 0.43 \pm 0.06\ M_\odot$. Kepler's Third law gives a distance between the mass centers of the stars of $1.99 \pm 0.01\ R_\odot$. The mean stellar densities were computed from Mochnacki's (1981) empirical relationship

$$\bar{\rho}_1 = \frac{0.0189}{(r_1^3\ (1 + q)\ P^2)} \text{ and } \bar{\rho}_2 = \frac{0.0189q}{(r_2^3\ (1 + q)\ P^2)}, \qquad (7)$$

where the stellar radius is normalized to the semi-major axis and P is in days. The computed values are $\bar{\rho}_1 = 2.30$ g cm^{-3} and $\bar{\rho}_2 = 1.74$ g cm^{-3}. The stellar radii, surface gravities, and bolometric magnitudes were calculated by the WD light curve program (LC). The visual luminosities of each star were calculated using the bolometric magnitudes from the LC output and the bolometric corrections from Pecaut and Mamajek (2013). The values for all the stellar parameters are reported in Table 4. The radii and masses are in good agreement with the mass and radius distribution of 112 contact binaries in a study by Gazeas and

Table 4. Provisional stellar parameters for PY Boo.

Parameter	*Symbol*	*Value*
Stellar masses	M_1 ($M_\odot$)	0.43 ± 0.06
	M_2 ($M_\odot$)	0.94 ± 0.06
Semi-major axis	a ($R_\odot$)	1.99 ± 0.01
Stellar radii	R_1 ($R_\odot$)	0.64 ± 0.01
	R_2 ($R_\odot$)	0.91 ± 0.02
Surface gravity	log g_1 (cgs)	4.46 ± 0.03
	log g_2 (cgs)	4.49 ± 0.06
Mean density	$\overline{\rho}_1$ (g cm^{-3})	2.30 ± 0.13
	$\overline{\rho}_2$ (g cm^{-3})	1.74 ± 0.09
Stellar luminosity	L_{1V} ($L_\odot$)	0.25 ± 0.02
	L_{2V} ($L_\odot$)	0.38 ± 0.04
Bolometric magnitude	$M_{bol,1}$	6.13 ± 0.09
	$M_{bol,2}$	5.59 ± 0.13

Values in this table are provisional (calculated). Radial velocity observations are necessary for direct determination of M_1, M_2, and a.

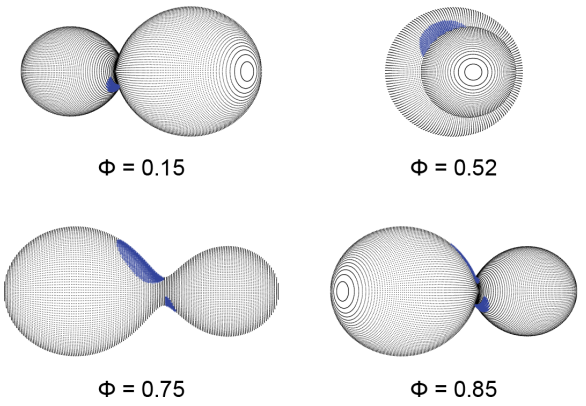

Figure 11. Roche Lobe surfaces of the best-fit WD spot model with orbital phase shown below each diagram.

Stępień (2008) (see their Figures 1–3). The geometrical and physical properties for those 112 stars were well determined. Two of their plots were reproduced in Figures 12 and 13 that also include the primary and secondary stars of PY Boo.

The third light contribution to the system light could possibly be another star orbiting the contact pair or an unresolved field star. The closest observed field star to PY Boo is located 35 arc seconds to the northwest. This star was well outside the annulus used in the photometric processing of the images, therefore it did not contribute to the third light measured. Assuming the third light source is a main-sequence star, its color can be estimated from the WD solution's g' and r' third light values. Converting the third light values to magnitudes gives a color of (g' – r') = 0.180 ± 0.008. Transforming this value using Equation 4 and correcting for color excess gives a color index of (B–V) = 0.378 ± 0.008. A main-sequence star of this color has an effective temperature of 6784 ± 46 K, a spectral type of F3V and a visual luminosity of L_{V3} = 4.9 ± 0.2 $L_\odot$ (Pecaut and Mamajek 2013). A star of this luminosity located in the PY Boo system would contribute 89% percent of the total system light (computed using L_{V1}, L_{V2} from Table 4 and L_{V3} above). This is much higher than the third light contribution found in the spotted WD solution whose values range from 21% – 27% for the g', r', and i' Sloan

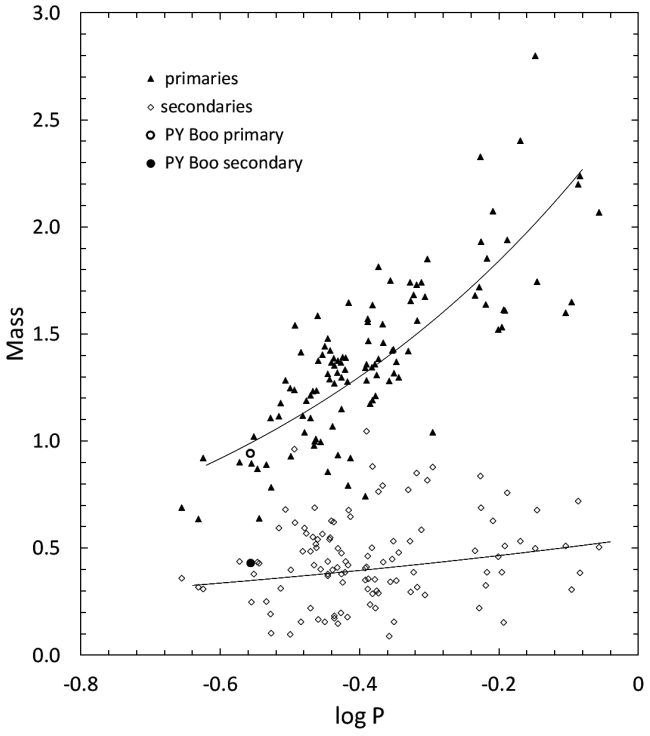

Figure 12. The mass distributions of 112 contact binaries with well determined geometrical and physical properties. The triangles are the primary star masses and the diamonds the secondary masses with PY Boo stars marked with the open and closed circles. The solid lines are the least-square fits from the analysis of Gazeas and Stępień (2008).

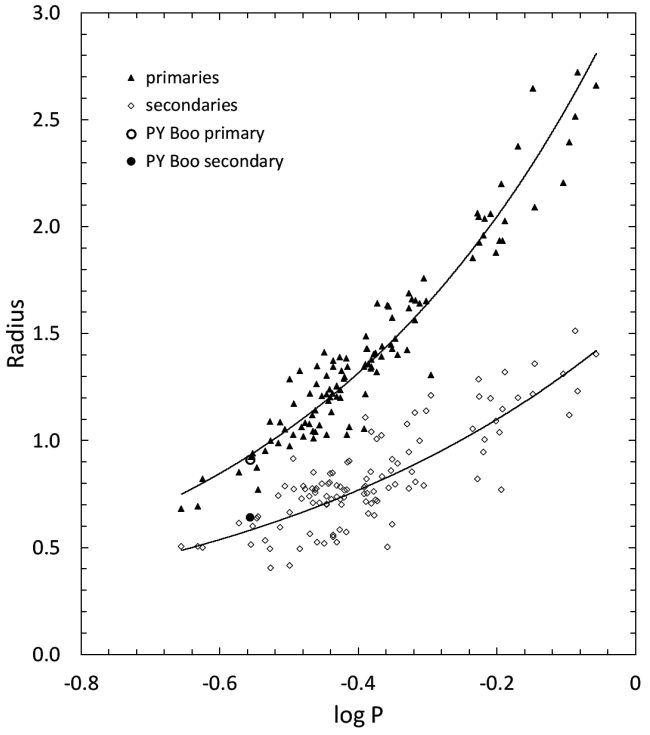

Figure 13. The radius distributions of 112 contact binaries with well determined geometrical and physical properties. The triangles are the primary star masses and the diamonds the secondary masses with PY Boo stars marked with the open and closed circles. The solid lines are the least-square fits from the analysis of Gazeas and Stępień (2008).

passbands (see Table 3). This result indicates the third light source is not in the PY Boo system but comes from a more distant unresolved field star.

The distance to PY Boo can be estimated from Ruciński and Duerbeck's (1997) luminosity calibration for contact binaries, which is based on HIPPARCOS parallaxes. This empirical relationship for absolute magnitude is given by

$$M_v = -4.44 \log_{10}(P) + 3.02 (B-V)_o + 0.12. \quad (8)$$

Substituting the orbital period and the (B–V) color index gives a value of $M_v = 5.37 \pm 0.22$ for the absolute magnitude. The apparent V-band magnitude at orbital phase $\varphi = 0.25$ was determined from the g' and r' magnitudes using Jordi *et al.*'s (2006) transformation equation which is given by

$$V = (-0.565 \pm 0.001)(g' - r') - (0.016 \pm 0.001) + g'. \quad (9)$$

The third light contribution was removed from the g' and r' magnitudes before substitution into Equation 9. This gives an apparent magnitude of $m_v = 12.53 \pm 0.01$. Correcting for extinction ($A_v = 0.05$) gives a distance modulus of $(m - M)_V = 7.11 \pm 0.22$ and a distance of 264 ± 27 pc.

As with many short period low mass contact binaries, PY Boo appears to be magnetically active. In this study, a number of light curves were obtained from different nights over a time span of 1 year. Noticeable changes were seen in the light curves over this time interval. At times Max I was brighter than Max II while at other times this reversed with Max II brighter than Max I (O'Connell effect). The observations used for the WD spotted solution had about equal maxima. In that solution the synthetic light curve did not fit the g' passband observations as well as the r' and i' passbands (see Figure 8). The g' band residuals in Figure 9 show a sinusoidal distribution. Since the g' observations were taken two weeks before the r' and i' observations it was suspected the spot configurations had changed over that two-week interval. To test this idea a new WD solution was attempted using only the g'-band observations with all stellar parameters held fixed at the spotted solution values (Solution 2). Only the light and spot parameters were allowed to vary. The initial spot parameter values were also taken from Solution 2. The resulting best-fit WD model for the g'-band observations is shown in column 4 of Table 3 (Solution 3). Figure 10 shows the improved model fit (solid line) with the bottom panel showing the residuals with the sinusoidal distribution no longer apparent. The most significant change in the spot configuration over the two-week interval was that the cool spot on the secondary star appears to have moved 9° in longitude and decreased in radius by 15%.

The decreasing orbital period reported in section 3 should be considered preliminary since the available set of minima times is small. A decreasing orbital period could be explained by magnetic braking. The rapidly changing spot configuration observed is a clear indication of magnetic activity in this binary. Angular momentum loss by magnetic braking was likely an important factor in bringing the stars into their current contact configuration (Stępień and Gazeas 2012). This process may be continuing at present time but may not be the only cause of the observed period change. With the stars in a contact configuration, conservative mass exchange from the larger more massive secondary star to the smaller hotter primary star could also be the cause of or contribute to the decreasing period. In this case the rate of mass transfer (Reed 2011) is given by

$$\frac{dM}{dt} = \frac{(\dot{P} M_1 M_2)}{3P(M_1 - M_2)}. \quad (10)$$

Substituting the rate of period change ($\dot{P}$) and the stellar masses gives a mass transfer rate of 2.3 (0.2) × 10^{-9} $M_\odot$ / day. It is also possible that the quadratic curve fit to the O–C data (Figure 4) is a small part of a sinusoidally varying ephemeris. This type of ephemeris would result from a third body in the system but the limited number of minima times does not support that supposition at this time.

PY Boo is a short period (P < 0.3 d) low mass contact binary. Model calculations by Stępień and Gazeas (2012) suggest it will remain in the contact phase for about 0.8 Gyr before eventually coalescing into single rapidly rotating star. A spectroscopic radial velocity study of this system combined with the photometric solution presented here would be invaluable in determining the absolute stellar parameters and providing insight into its current evolutionary state. New times of minima light with observations spread over several years would also be invaluable in confirming the decreasing orbital period and provide evidence for a third star if one exists.

6. Acknowledgements

This research was made possible through the use of the AAVSO Photometric All-Sky Survey (APASS), funded by the Robert Martin Ayers Sciences Fund. This research has made use of the SIMBAD database, operated at CDS, Strasbourg, France.

References

Bradstreet, D. H., and Steelman, D. P. 2002, *Bull. Amer. Astron. Soc.*, **34**, 1224.

Diethelm, R. 2012, *Inf. Bull. Var. Stars*, No. 6029, 1.

Gazeas, K., and Stępień, K. 2008, *Mon. Not. Roy. Astron. Soc.*, **390**, 1577.

Gettel, S. J., Geske, M. T., and McKay, T. A. 2006, *Astron. J.*, **131**, 621.

Henden, A. A., *et al.* 2014, AAVSO Photometric All-Sky Survey, data release 9 (http://www.aavso.org/apass).

Hoffman, D. I., Harrison, T. E., and McNamara, B. J. 2009, *Astron. J.*, **138**, 466.

Hoňková, K. *et al.* 2014, *Open Eur. J. Var. Stars*, No. 165, 1.

Hübscher, J. 2013b, *Inf. Bull. Var. Stars*, No. 6084, 1.

Hübscher, J. 2015b, *Inf. Bull. Var. Stars*, No. 6152, 1.

Hübscher, J. 2016, *Inf. Bull. Var. Stars*, No. 6157, 1.

Hübscher, J., and Lehmann, P. 2013a, *Inf. Bull. Var. Stars*, No. 6070, 1.

Hübscher, J., and Lehmann, P. 2015a, *Inf. Bull. Var. Stars*, No. 6149, 1.

Jester, S. *et al.*, 2005, *Astron. J.*, **130**, 873.

Jordi, K., Grebel, E. K., and Ammon, K. 2006, *Astron. Astrophys.*, **460**, 339.
Kafka, S. 2016, variable star observations from the AAVSO International Database (https://www.aavso.org/aavso-international-database
Lucy, L. B., 1968, *Astrophys. J.*, **151**, 1123.
Lucy, L. B., and Wilson, R. E. 1979, *Astrophys, J.*, **231**, 502.
Luo, A-Li, *et al.* 2015, *Res. Astron. Astrophys.*, **15**, 1095.
Mirametrics 2015, Image Processing, Visualization, Data Analysis (http://www.mirametrics.com).
Mochnacki, S. W. 1981, *Astrophys. J.*, **245**, 650.
Paschke, A. 2014, *Open Eur. J. Var. Stars*, No. 162, 1.
Pecaut, M. J., and Mamajek, E. E. 2013, *Astrophys. J., Suppl. Ser.*, **208**, 9 (http://www.pas.rochester.edu/~emamajek/EEM_dwarf_UBVIJHK_colors_Teff.txt).
Qian, S. 2003, *Mon. Not. Roy. Astron. Soc.*, **342**, 1260.
Reed, P. A. 2011, in *Mass Transfer Between Stars: Photometric Studies, Mass Transfer—Advanced Aspects*, ed. H. Nakajima, InTech DOI: 10.5772/19744. (http://www.intechopen.com/books/mass-transfer-advanced-aspects/mass-transfer-between-stars-photometric-studies).
Ruciński, S. M. 1969, *Acta Astron.*, **19**, 245.
Ruciński, S. M., and Duerbeck, H. W. 1997, *Publ. Astron. Soc. Pacific*, **109**, 1340.
Stępień, K., and Gazeas, K. 2012, *Acta Astron.*, **62**, 153.
Terrell, D., and Wilson, R. E. 2005, *Astrophys. Space Sci.*, **296**, 221.
Van Hamme, W. 1993, *Astron. J.*, **106**, 2096.
Van Hamme, W., and Wilson, R. E. 1998, *Bull. Amer. Astron. Soc.*, **30**, 1402.
Willingale, R., Starling, R. L. C., Beardmore, A. P., Tanvir, N. R., and O'Brien, P. T. 2013, *Mon. Not. Roy. Astron. Soc.*, **431**, 394, (http://www.swift.ac.uk/analysis/nhtot/).
Wilson, R. E. 1978, *Astrophys. J.*, **224**, 885.
Wilson, R. E., and Biermann, P. 1976, *Astron. Astrophys.*, **48**, 349.
Wilson, R. E., and Devinney, E. J. 1971, *Astrophys. J.*, **166**, 605.
Wozniak, P. R., *et al.* 2004, *Astron. J.*, **127**, 2436.